Numerical study of laminar-turbulent transition in particle-laden channel flow

Joy Klinkenberg,[1,2] Gaetano Sardina,[2,3] H. C. de Lange,[1] and Luca Brandt[2]
[1]*TU/e, Mechanical Engineering, 5600 MB, Eindhoven, The Netherlands*
[2]*Linné Flow Centre, KTH Mechanics, S-100 44 Stockholm, Sweden*
[3]*School of Engineering and Architecture, University of Enna Kore, Enna, 94100, Italy*
(Received 13 May 2012; revised manuscript received 26 October 2012; published 23 April 2013)

We present direct numerical simulations of subcritical transition to turbulence in a particle-laden channel flow, with particles assumed rigid, spherical, and heavier than the fluid. The equations describing the fluid flow are solved with an Eulerian mesh, whereas those describing the particle dynamics are solved by Lagrangian tracking. Two-way coupling between fluid and particles is modeled with Stokes drag. The numerical code is first validated against previous results from linear stability: the nonmodal growth of streamwise vortices resulting in streamwise streaks is still the most efficient mechanism for linear disturbance amplification at subcritical conditions as for the case of a single phase fluid. To analyze the full nonlinear transition, we examine two scenarios well studied in the literature: (1) transition initiated by streamwise independent counter-rotating streamwise vortices and one three-dimensional mode and (2) oblique transition, initiated by the nonlinear interaction of two symmetric oblique waves. The threshold energy for transition is computed, and it is demonstrated that for both scenarios the transition may be facilitated by the presence of particles at low number density. This is due to the fact that particles may introduce in the system detrimental disturbances of length scales not initially present. At higher concentrations, conversely, we note an increase of the disturbance energy needed for transition. The threshold energy for the oblique scenario shows a more significant increase in the presence of particles, by a factor about four. Interestingly, for the streamwise-vortex scenario the time at which transition occurs increases with the particle volume fraction when considering disturbances of equal initial energy. These results are explained by considering the reduced amplification of oblique modes in the two-phase flow. The results from these two classical scenarios indicate that, although linear stability analysis shows hardly any effect on optimal growth, particles do influence secondary instabilities and streak breakdown. These effects can be responsible of the reduced drag observed in turbulent channel flow laden with heavy particles.

DOI: 10.1103/PhysRevE.87.043011 PACS number(s): 47.20.Ft, 47.55.Kf

I. INTRODUCTION

Laminar-turbulent transition in shear flows has been studied extensively in the past [1], but it is still not fully understood. Transition leads to an increase of the drag and is therefore often undesirable. One possible way to influence the transition scenario is by suspending additives in the flow, as it is shown that turbulent drag can be reduced by small amounts of, e.g., polymers [2], rigid fibers [3], or small heavy particles [4–7], as investigated here. Although many fluid flows of practical interest are seeded with particles, our knowledge about the influence of particles on the flow, in particular on laminar-turbulent transition, is still limited. Most studies concern particle-laden turbulent flows; see the reviews by Toschi and Bodenschatz [8] and Balachandar and Eaton [9].

A particle in a fluid flow is subject to several different interaction forces [10]. First, the drag force between the particle and the fluid: when the particle and fluid have slightly different velocities a shear force is present. Furthermore, there are added mass and pressure forces, as well as history effects. For larger particle volume fraction, particle-particle interactions also have to be taken into account. This suggests the complexity and richness of the phenomena occurring in particle-laden flows.

Linear stability analysis is typically considered the first step towards understanding transition to turbulence. This allows the determination of critical values of the relevant adimensional parameters above which exponentially growing disturbances exist. However, in many configurations, e.g., shear flows, transition is subcritical, and a full nonlinear analysis is needed. In these flows, it is still possible to show that linear mechanisms are responsible for the instantaneous amplification of perturbation energy, and therefore a linear nonmodal analysis [1] can reveal the mechanisms responsible for transition in linearly stable cases. This was the case with the linear lift-up process that was identified as a key process in wall-bounded flows. Indeed, subcritical transition in shear flows is associated to the presence of streamwise elongated structures, the so-called streaks.

Previous investigations of laminar-turbulent transition with the inclusion of particles are performed by Matas *et al.* [11,12]. These authors carried out experiments on particle-laden flows using neutrally buoyant particles in a pipe flow. To control transition to start at Re $\approx$ 2100 for a clean flow, they inserted a ring at the pipe entrance. Particles of four different sizes were injected into the flow, and the Reynolds number at which the transition starts, the transitional Reynolds number, recorded. They found that for large concentrations all particle sizes stabilized the flow, i.e., the transitional Reynolds number increased. For smaller concentrations (volume fraction $\leqslant 0.2$), large particles destabilized the flow, while the smaller particles ($d/D \leqslant 70$) stabilized the flow. Interestingly, in the range of small particles, the results became independent of the particle diameter.

In our previous work [13,14], the linear stability of flows seeded with either heavy or light particles was investigated. For a flow with heavy particles only, the Stokes drag needs

to be taken into account. For a flow with light particles, added mass and fluid acceleration also need to be included. We have shown that particles do not influence the transient growth of disturbances in plane channel flow. The optimal initial disturbances consist of counterrotating streamwise vortices forming streamwise-independent streamwise velocity perturbations, the streaks, as for single-phase fluids. This finding was explained by the fact that the time scale associated with the transient growth of the streaks is larger than the typical particle relaxation time so that heavy particles effectively act just to enhance the suspension density. This suggested that the initial linear stages of transition may not be affected by the presence of particles. However, experiments [4,6] and numerical simulations [7] demonstrate that adding heavy particles reduces the drag of a turbulent channel flow. As an example, the experiments in Ref. [6] consider the pipe flow of glass particles in air at a Reynolds number between 10 000 and 20 000 and mass load up to 1.5. The reduction of the wall shear stress is measured to be as high as 30%. The latter result indicates that particles have an effect on turbulent structures. Therefore, although particles show no influence in the initial linear stages of transition, they might have an effect on secondary, nonlinear, instabilities. The aim of the present paper is therefore to investigate the effect of rigid, spherical particles on the evolution of finite-size disturbances leading to turbulent flow.

To investigate this effect, we use direct numerical simulations of a plane Poiseuille flow extended with a model for two-way coupling between the particles and fluid using Stokes drag as interaction force. Gravitational forces are initially neglected; indications about the effect of gravity are provided in an appendix and in-depth analysis left for future work. We study the behavior of a finite energy perturbation, instead of infinitesimal small perturbations as in linear stability analysis. We investigate how the threshold energy for transition, the minimum initial disturbance energy necessary to reach the turbulent state, varies in the presence of heavy particles as well as how the solid phase changes the evolution of disturbances of given initial shape and amplitude. This provides information about the nonlinear behavior of streaks, and it shows whether the secondary instabilities might be damped by the presence of particles.

In relation to energy thresholds in subcritical transition several researchers have considered the concept of "edge of chaos" [15]. This is the asymptotic state reached by perturbations, neither decaying to a laminar state nor evolving to turbulence. Near the "edge of chaos," exact coherent structures are found [16–18]. The dynamics on the laminar turbulent boundary have been investigated more recently by several groups [15,19–23]. A review is given in Ref. [24].

Exact coherent structures are also reported for dilute polymer solutions in Ref. [25] for plane Couette flow. These authors found that these exact solutions are a promising method for capturing the essential physics of drag reduction in polymer suspensions. More recently, the numerical simulations by Xi and Graham [26,27] of drag-reducing polymer solutions in the parameter regime close to laminar-turbulent transition reveal intervals of hibernating (low-activity) turbulence characterized by weak streamwise vortices and nearly nonexistent streamwise variations.

In this paper we examine two transition scenarios previously analyzed as representative of subcritical transition; see, e.g., Ref. [28]. First, we consider a transition initiated by streamwise vortices (SVs), without any streamwise dependence. SVs trigger the largest linear transient growth and are common in many shear flows [29,30]. Following Ref. [28], the transition process initiated by these vortices can be summarized as

$$\begin{aligned}\text{streamwise vortices} &\Rightarrow \text{streamwise streaks}\\ &\Rightarrow \text{streak breakdown} \Rightarrow \text{transition}.\end{aligned}$$

Because transition cannot take place with only streamwise-independent structures, one needs to consider streamwise-dependent traveling perturbations able to trigger streak breakdown and transition. Here we choose not to examine the effect of background noise, but introduce a time-periodic oblique-mode of given amplitude. Indeed Schoppa and Hussain [31] and Cossu *et al.* [32] show how simple spanwise modulations of the streak can induce a rapid breakdown.

In the second route to turbulence discussed in Ref. [28], we consider at time zero a pair of oblique optimal waves (OW scenario). Each of these waves grows by a nonmodal mechanism so that they can nonlinearly interact. From this quadratic interaction, streamwise-independent SVs are formed that in turn induce streamwise streaks via the lift-up effect. The following breakdown is thus similar to the SV scenario discussed above:

$$\begin{aligned}\text{oblique waves} &\Rightarrow \text{streamwise vortices}\\ &\Rightarrow \text{streamwise streaks} \Rightarrow \text{streak breakdown}\\ &\Rightarrow \text{transition}.\end{aligned}$$

The details of this scenario have been extensively investigated in the past for a clean fluid flow; see, e.g., Refs. [33–35]. Note that the oblique scenario is found to be the most efficient way to trigger turbulence (see Refs. [19,28]), and it can be identified also in nonlinear optimal localized initial conditions [36,37].

The paper is organized as follows. First, we present the governing equations and the details of our numerical implementation. Second, we validate the numerical code against the data from linear theory presented in Ref. [13]. Later we report the results for the two scenarios described above when varying the particle mass fraction, and we conclude the paper with a summary and a discussion of the main findings.

II. GOVERNING EQUATIONS AND IMPLEMENTATION

A. Governing equations

The equations of motion for the fluid are modeled in an Eulerian grid, whereas the particles are evolved in a Lagrangian framework. The particles are assumed to be rigid spheres heavier than the carrier phase with a diameter smaller than the smallest flow characteristic length scale. By neglecting gravity, under the assumption of heavy particles, the only significant force acting on a single particle is the Stokes drag [10]. The

equations in nondimensional form are

$$\frac{\partial u_i}{\partial x_i} = 0, \tag{1}$$

$$\frac{\partial u_i}{\partial t} = -\frac{\partial p}{\partial x_i} - u_j \frac{\partial u_i}{\partial x_j} + \frac{1}{R}\frac{\partial^2 u_i}{\partial x_j^2} + \sum_p \frac{f}{SR}(u_{p_i} - u_i) \times \left(1 + 0.15\mathrm{Re}_p^{0.687}\right)\delta(x_i - x_{p_i}), \tag{2}$$

$$\frac{dx_{p_i}}{dt} = u_{p_i}, \tag{3}$$

$$\frac{du_{p_i}}{dt} = \frac{u_i - u_{p_i}}{SR}\left(1 + 0.15\mathrm{Re}_p^{0.687}\right), \tag{4}$$

where u_i is the fluid velocity and u_{p_i} the velocity of one particle. In the equations above, δ is the Dirac delta function, f the mass fraction of particles, the Reynolds number $R = UL/\nu$, and $SR = \tau_p \frac{U}{L}$ the Stokes number defined using the convective time scale of the flow with L the channel half-width and U the laminar centerline velocity. The particle relaxation is defined as $\tau_p = \frac{2}{9}\frac{r^2}{\nu}\frac{\rho_p}{\rho_f}$, with r the radius of the particle, ρ_p the density of the particle, ρ_f the fluid density, and ν the kinematic viscosity. The nonlinear formulation of the Stokes drag is employed to account for a small but finite particle Reynolds number $\mathrm{Re}_p = |u - u_p|2r/\nu$. Here we follow the formulation described in [38] with drag coefficient for the sphere $C_D = 24/\mathrm{Re}_p(1 + 0.15\mathrm{Re}_p^{0.687})$.

The Stokes number is a dimensionless relaxation time multiplied by the Reynolds number. This dimensionless relaxation time is based on the flow viscous time scale and defined as $S = \frac{\nu\tau_p}{L^2} = \frac{2r^2\rho_p}{9L^2\rho_f}$; therefore it is only a function of particle size and density ratio. Here we set the density ratio to $\xi = \rho_f/\rho_p = 0.001$; i.e., we assume that the carrier phase is air. In this way, we can directly relate the size of the particles to the relaxation time. The size of the particles can be related to the number of particles (N) using the volume fraction (Φ):

$$\Phi = f\xi, \quad N = \frac{\Phi}{4/3\pi r^3}.$$

B. Implementation

The numerical code is an efficient pseudospectral solver for the three-dimensional incompressible Navier-Stokes equations with a particle-tracking algorithm for the solid phase. The velocity components of the fluid phase are expanded in both x (streamwise) and z (spanwise) direction with Fourier modes and with Chebyshev polynomials in the wall-normal, or y direction. To advance Eq. (2) in time, we use a fourth-order Runge-Kutta algorithm. Periodic boundary conditions are assumed in x and z with no slip at both walls, $y = \pm 1$. More details about the code are given in Ref. [39].

The particles are evolved by means of a Lagrangian Solver and are coupled to the Eulerian grid of the fluid flow [40]. The fluid velocities are interpolated from the Eulerian grid onto the particle positions using a trilinear interpolation. The time advancement of the particle uses the same Runge-Kutta algorithm as the time advancement of the fluid. The Stokes drag, also forcing the momentum equation, can be extrapolated back onto the Eulerian grid using the same trilinear scheme of the interpolation. The particle back reaction is calculated in physical space and added to the nonlinear term, before Fourier transformation back into spectral space. For a review of the numerical procedure to model the particle back reaction on the flow see Refs. [41,42].

C. Flow configuration and resolution

We study a plane Poiseuille flow given as base velocity by imposing a constant mass flux. The streamwise and spanwise dimensions of the domain are $L_x = 2\pi$ and $L_z = 2\pi$, with $L_y = 2$ the channel width. The Reynolds number used in all computations is 2000. If we consider air, typical velocity are of the order of meters per second and typical lengths of the order of the centimeters. The resolution used is typically $64 \times 65 \times 64$ for streamwise, wall-normal, and spanwise directions, respectively. Several resolutions have been used to investigate the convergence of the solution [43]. If the flow reaches the turbulent state in our configuration, the friction Reynolds number $\mathrm{Re}_\tau = U_\tau h/\nu = 93$ with U_τ the friction velocity. In these conditions, the grid size in friction wall-units $\delta^+ = \nu/U_\tau$ becomes $\Delta_x^+ = \Delta_z^+ = 6.5$ and $\Delta_y^+ = 0.12$–5 with seven grid points inside the viscous layer. This mesh can be considered more than enough for a good DNS of a turbulent channel flow [44].

A bisection algorithm is used to find the energy threshold for transition [19,23,45]. The criterion for convergence of the energy threshold is the following:

$$2\frac{A_t - A_l}{A_t + A_l} < 1 \times 10^{-5},$$

where A_t and A_l are the smallest and largest amplitudes at which turbulent and laminar flow are observed.

III. RESULTS

In Sec. III A the numerical implementation is validated against the linear stability results in Ref. [13], obtained under the continuum assumption. Transition initiated by streamwise-independent counterrotating streamwise vortices and a weak three-dimensional disturbance is analyzed in Sec. III B. We aim to identify the threshold energy of the initial condition: A slightly lower amplitude will result in laminar flow, while a slightly larger amplitude in a turbulent flow. Results for the oblique scenario are presented in Sec. III C. Finally we will look at particle concentration and accumulation during the transition process. By isolating two different mechanisms for streak formation and breakdown, ingredients of the self-sustaining cycle underlying wall-bounded turbulence, we wish to also understand the effects of the dispersed solid phase in the turbulent regime.

A. Linear evolution

We consider as initial condition a Poiseuille flow with a low-amplitude disturbance of spanwise wave number $\beta = 2$ and streamwise wave number $\alpha = 0$. This initial disturbance is the linear optimal initial condition yielding the largest energy growth over time and over disturbances of different wave number and consists of streamwise vorticity. Particles are assumed to have the same initial velocity as the undisturbed base flow and to be uniformly distributed. Figure 1(a) shows

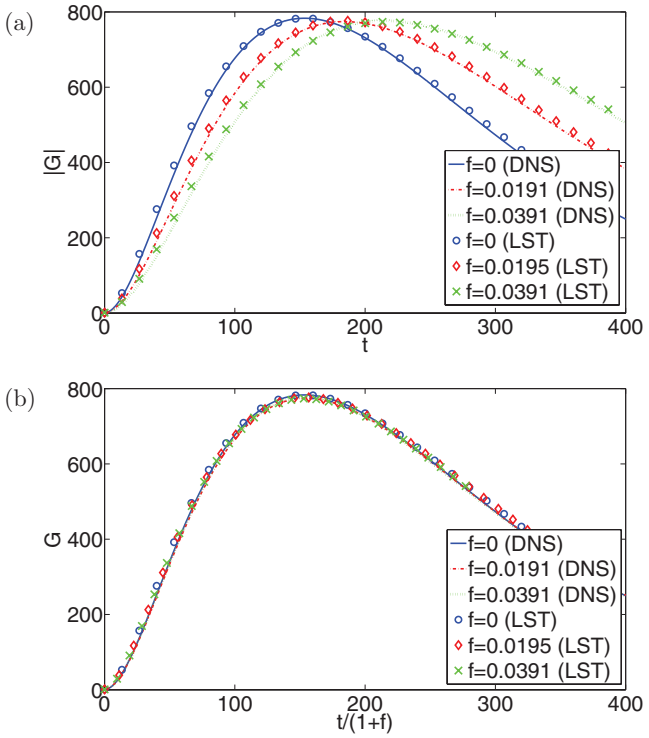

FIG. 1. (Color online) Transient energy growth of disturbances with streamwise and spanwise wave numbers $(\alpha,\beta) = (0,2)$, $SR = 5$, and $R = 2000$ versus time. (a) Comparison between linear stability theory (LST) and DNS. (b) Energy growth versus time divided by $(1 + f)$ to show the scaling of the time of optimal growth.

the time evolution of the disturbance energy for $SR = 5$ and two values of the mass fraction f: We compare results from linear stability and from our numerical implementation where a low initial amplitude is chosen to have a linear disturbance behavior. We observe the transient growth of streamwise velocity streaks forced by the initial streamwise vortices before the perturbation energy eventually goes to zero. These results show that we correctly reproduce by direct numerical simulation the linear nonmodal results in Ref. [13]. Linear stability analysis predicts that for initial disturbances consisting only of fluid velocity particles affect only the time needed to reach the maximum growth; the growth itself is hardly affected. The time at which the energy maximum is observed is delayed by a factor $(1 + f)$. This is confirmed in Fig. 1(b), where the energy amplification is shown for several values of f and time divided by $(1 + f)$.

B. Streak scenario

To study the full nonlinear transition we consider the initial perturbation introduced above (streamwise-independent vortices) and two different additional streamwise-dependent disturbances of wave vector $(\alpha = 1,\ \beta = 1)$ for the case denoted SV1 and $(\alpha = 1,\ \beta = 2)$ for the case SV2. The oblique mode is necessary to trigger transition in a controlled and reproducible way since it introduces a three-dimensional velocity field. In our simulations, this oblique mode has an initial energy equal to 1/9 of that pertaining to the streaky (0,2) mode, a value close to the optimal found in Ref. [19].

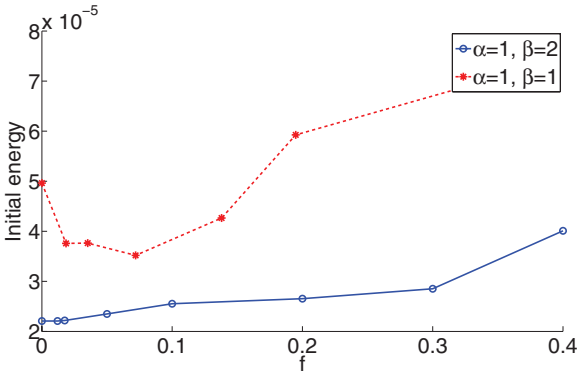

FIG. 2. (Color online) The critical threshold energy as a function of the particle mass fraction f for the SV scenario initiated by streaks and two different oblique waves $(\alpha = 1,\beta = 1)$ (denoted SV1) and $(\alpha = 1,\beta = 2)$ (SV2); $SR = 5$ and $R = 2000$.

The energy threshold for transition is shown in Fig. 2 versus the particle mass fraction. We first notice that the scenario SV2 has a lower energy threshold for transition. The global minimum energy threshold is slightly increasing in the presence of particles; at small mass fractions the disturbance energy needed to reach turbulence is smaller than in a clean fluid flow for SV1, whereas it is monotonically increasing for SV2. At larger mass fractions an increased threshold energy is found in both cases. Note also that the threshold curves for transition have usually a fractal or complicated behavior; they are sensitive to the specific initial condition. For the present case, critical energy amplitudes are not found to vary in a noticeable manner when initiating the particles with the local fluid velocity instead of the base flow velocity.

Besides the effect of the solid phase on the threshold energy just discussed, Fig. 3 reveals that the time at which transition occurs is altered by the presence of heavy particles. Here we report the time evolution of the integrated wall-normal v and streamwise u fluid velocity perturbations for flows with different particle mass fractions for the scenario SV1, where the disturbance velocity is defined as the fluid velocity minus the base flow parabolic profile. In all cases we kept constant the initial disturbance energy at 6.25×10^{-5}. The transition follows a similar path in all cases displayed, although the time at which transition is observed (identified by the sharp increase of the wall-normal velocity perturbation) is increasing by a factor of three or more in the presence of particles. Note that for the particular amplitude chosen here the flow stays laminar for a mass fraction $f = 0.39$; however, the trend reported is observed to be independent of the particular value of the initial disturbance energy. The data also reveal that the amplitude of the streamwise velocity disturbances is constant when varying the mass fraction f, and therefore the transient growth of the streaks is not affected by the presence of particles, as predicted by linear theory [see Fig. 1(b)]. The same trend is observed for the scenario SV2, therefore not shown here, although the transition time is delayed only by a factor two.

To better follow the disturbance evolution during transition we report in Fig. 4 the energy pertaining to selected modes of given streamwise and spanwise wave number (α,β) versus time for a low and a high value of the mass fraction f. In each plot dotted lines indicate the energy evolution in the case of

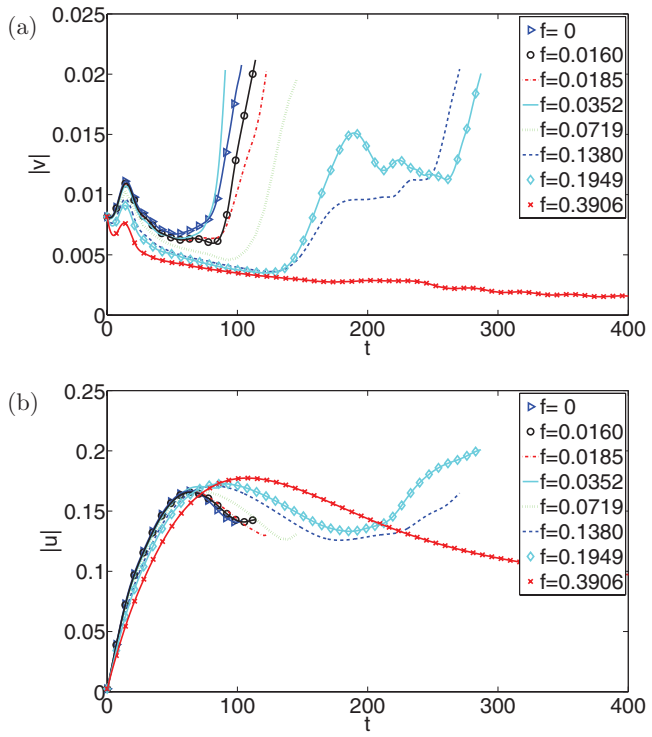

FIG. 3. (Color online) Volume integral of the wall-normal velocity v (a) and streamwise velocity u (b) of the perturbation as a function of time for $SR = 5$ and $R = 2000$ and the values of the mass fraction f reported in the legend. The initial perturbation energy is 6.25×10^{-5}.

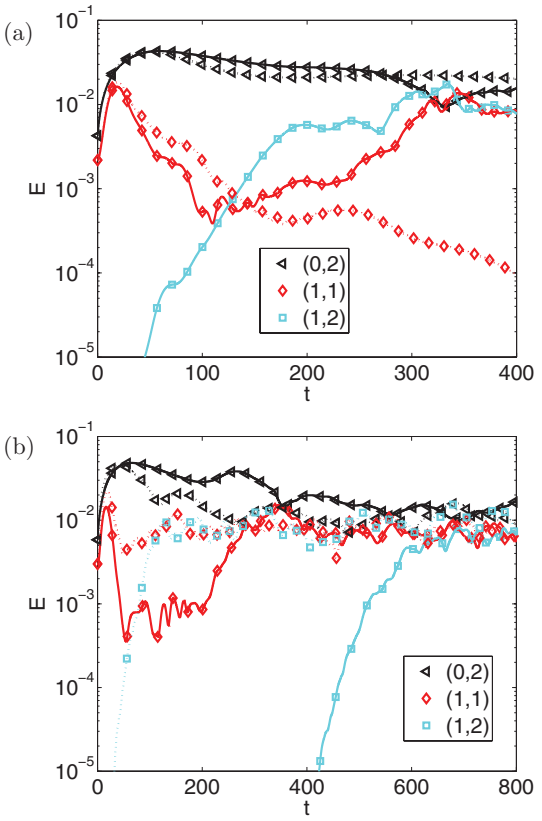

FIG. 4. (Color online) Time evolution of the disturbance energy for the SV1 scenario and three Fourier modes ($\alpha = 0, \beta = 2$), (1,1) and (1,2). (a) Low mass fraction $f = 0.07$ and initial energy $E_0 = 4 \times 10^{-5}$. (b) High mass fraction $f = 0.39$ and initial energy $E_0 = 7.5 \times 10^{-5}$. In each plot dotted lines indicate the energy evolution in the case of single phase fluid for the same initial conditions.

single phase fluid for the same initial conditions. The data are shown for SV1 where the transition delay is more evident, as well as to be able to explain the initial decrease in threshold energy evident in Fig. 2.

The initial increase of the magnitude of the ($\alpha = 1$, $\beta = 1$) mode, as well as the wall-normal velocity disturbance in Fig. 3(a), displays the initial weak transient growth of the oblique modes. The data clearly indicate that the amplitude of the oblique mode decreases for increasing mass fraction f, while the streaks [(0,2) mode] are hardly affected by the presence of the particles. Figure 4(a) reveals that the (1,2) mode is responsible for the decrease of disturbance energy threshold at low mass fraction. This mode is observed only in the presence of particles and is created by the localized forcing from the particles to the flow. Indeed, the (1,2) mode cannot be generated by nonlinear interactions between the (1,1) and (0,2) modes only. This fundamental (1,2) mode is most detrimental for the streak instability that is therefore initiated at lower disturbance amplitudes. The results in Fig. 4(b) indicate that the (1,2) mode is not induced as efficiently at large mass fraction, and the transition is therefore delayed because the background noise level given by the oblique modes is weaker. Note also that when introducing directly the (1,2) mode into the flow (Fig. 2), transition is monotonically delayed: particles are not able to introduce perturbation that can be more dangerous than those already present.

To confirm our explanation, we examine the linear behavior of the (1,1) and (1,2) modes. The linear optimal growth is given in Fig. 5 where the largest possible transient energy growth, maximized over all possible final times at which the disturbance is measured, is displayed versus the mass fraction f for $SR = 5$ and, in the inset, versus the particle Stokes number SR for different values of the mass fraction f. The figure illustrates that a larger mass fraction decreases

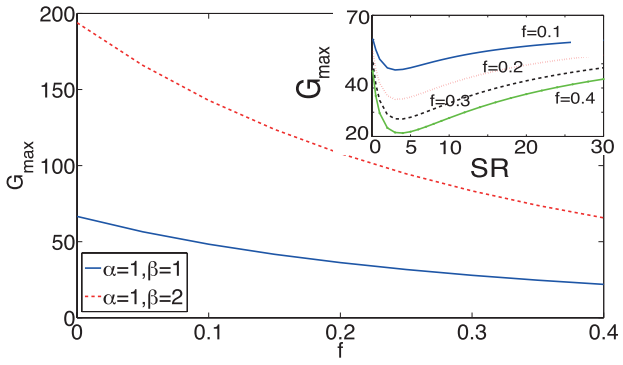

FIG. 5. (Color online) Optimal growth of the oblique mode ($\alpha = 1$, $\beta = 1$) and ($\alpha = 1$, $\beta = 2$) versus the mass fraction f for $SR = 5$ and $R = 2000$. The inset displays the optimal growth versus Stokes number SR for the indicated values of the mass fraction f and mode ($\alpha = 1$, $\beta = 1$). The optimal energy gain is maximized over all possible final times.

the optimal growth significantly and that minimum transient growth is observe for $SR \approx 4$; the value considered in this study is therefore representative of conditions at which the particle size has a noticeable effect. Here we consider the singular values of the system as representative of the behavior of the oblique modes, and we can therefore conclude that particles stabilize the oblique mode and this induces a delay of the time at which transition is observed. This is associated to a less effective start of the streak disruption. As a consequence, given the significant delay of the time of transition, one can speculate that more persistent streaks would be observed in a noisy environment, a situation reminiscent of the hibernating phases on the edge trajectories identified by Xi and Graham [26] in dilute polymer solutions.

In the light of the above discussion, we can now interpret the energy threshold reported in Fig. 2. The initial decay of the energy reported for the SV1 scenario at low values of the concentration can be attributed to the extra forcing from the particles to the fluid, with particles acting at more isolated locations. This forcing initiates slightly more efficiently the streak breakdown. This is, however, not a general conclusion, and the same phenomenon is not observed for SV2 at low f when the most dangerous mode for streak instability is forced in a controlled manner. In both scenarios, at larger values of f we observe a stabilizing effect: the amplitude of the oblique mode introduced initially decreases faster, and its action is less detrimental.

In summary, for the scenario considered here, streaks need to reach a sufficient high amplitude so that secondary instabilities can initiate; this streak generation process is hardly changed by the particles. However, oblique modes are generally weakened by the solid phase, and this induces a transition delay since the time for transition does depend on the amplitude of the streamwise-dependent forcing induced by the particles and the oblique mode. The delay can therefore be explained by the fact that the oblique modes determining the initial amplitude of the growing secondary instability mode becomes weaker in the presence of particles.

C. Oblique scenario

As discussed above, the oblique OW scenario is initiated by a pair of symmetric oblique waves, ($\alpha = 1$, $\beta = \pm 1$). These waves interact nonlinearly and initiate streaks of wave vector (0,2) in the flow, as in the scenario examined in the previous section [28]. The two oblique waves are both given the same initial energy, and again particles are initialized uniformly distributed and with zero disturbance velocity (simulations where particles have initially the local fluid velocity gave no significant differences in the results).

The threshold energy for transition is displayed in Fig. 6 versus the particle mass fraction. As in the previous scenario, the energy required to reach the turbulent state decreases at low mass fraction and then increases with f; in this case, however, the increase of the threshold energy is more significant, approximately by a factor four for the largest mass fractions considered. As discussed for the SV scenario, we attribute the initial decrease of the energy required to transition to the modulation introduced in the system by the few particles present. The largest increase observed at large f is instead

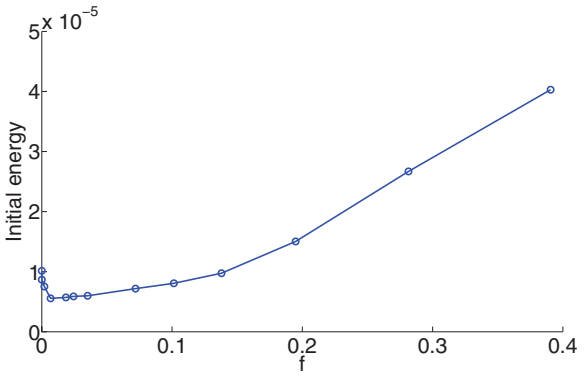

FIG. 6. (Color online) The critical threshold energy for the OW scenario initiated by two symmetric oblique waves ($\alpha = 1$, $\beta = \pm 1$) as a function of the particle mass fraction f with $SR = 5$ and $R = 2000$.

related to the decreased amplitude of the oblique modes in the presence of particles, as also discussed above in relation to Fig. 5.

The time evolution of the integral of the perturbation velocities is reported in Fig. 7 for initial disturbances of energy 8×10^{-6}. Such a relatively low amplitude has been show to highlight how, unlike in the SV scenario, the streak amplitude is significantly reduced when increasing the particle mass fraction. Indeed, Fig. 7(b) displays a monotonic decrease of the streak amplitude when increasing f. The transient growth of the streaks is significantly delayed by the lower amplitude of the interacting oblique modes. In addition, in contrast to the case of transition initiated by a pair of counterrotating

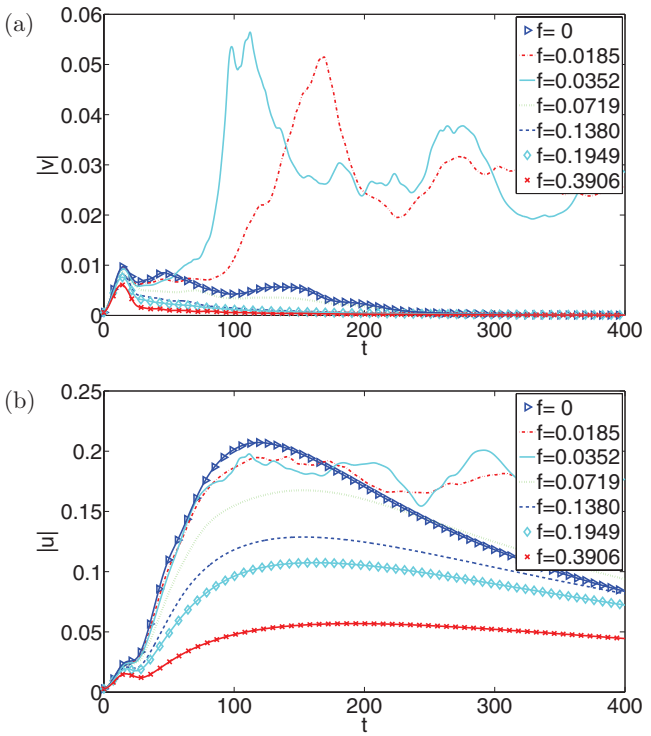

FIG. 7. (Color online) The v velocity (a) and u velocity (b) as a function of time for several mass fractions at $SR = 5$ and $R = 2000$ with an initial perturbation energy of 8×10^{-6}.

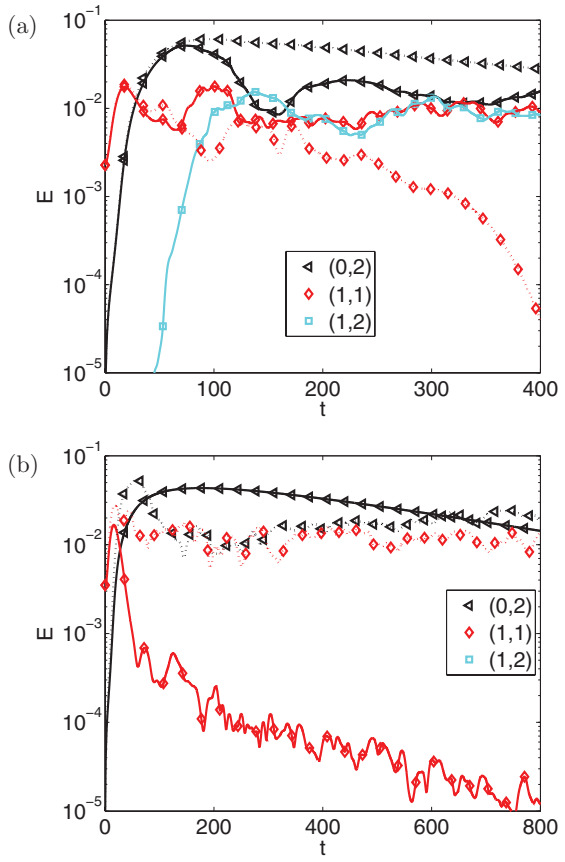

FIG. 8. (Color online) Time evolution of the disturbance energy for the OW scenario and three Fourier modes ($\alpha = 0$, $\beta = 2$), (1,1) and (1,2). (a) Low mass fraction $f = 0.035$ and initial energy $E_0 = 8.7 \times 10^{-6}$. (b) High mass fraction $f = 0.39$ and initial energy $E_0 = 2.1 \times 10^{-5}$. In each plot dotted lines indicate the energy evolution in the case of single phase fluid for the same initial conditions. The oblique mode $(1, -1)$ has the same energy levels as its symmetric counterpart (1,1).

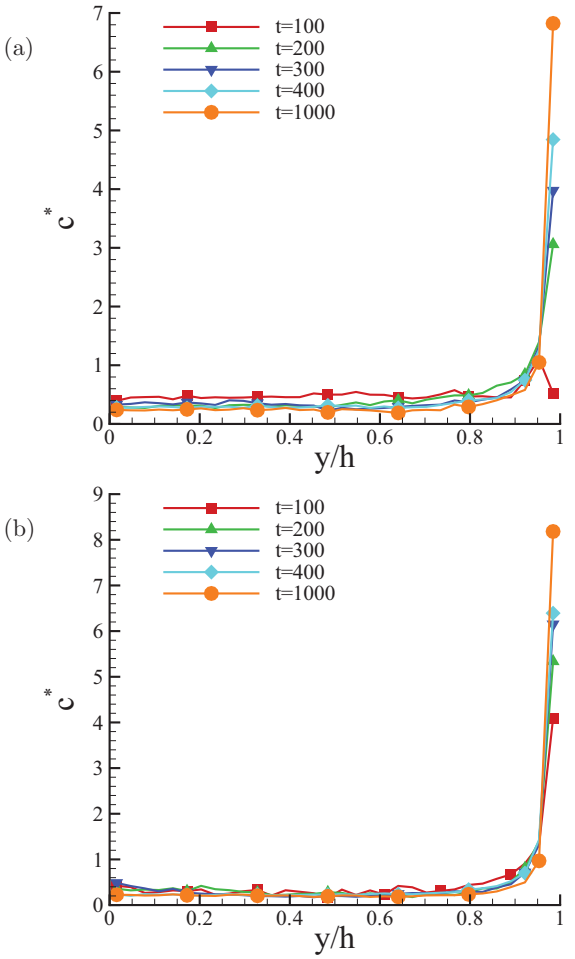

FIG. 9. (Color online) Time evolution of normalized particle concentration for (a) SV1 scenario and (b) OW scenario for particle mass fraction $f = 0.02$ and initial amplitude just above the threshold for transition to turbulence. $SR = 5$ and $R = 2000$. Transition to turbulence occurs at $t \approx 100$ for SV and $t \approx 80$ for OW.

streamwise vortices, there is no significant time delay in the transition for values of the initial energy above the critical threshold (see Ref. [43]).

The energy of single Fourier components in the flow is depicted in Fig. 8 for two different values of the mass fraction f. From the figures one can also appreciate the steps involved in the oblique transition: first, the amplification of the oblique modes [see also v perturbation at $t \approx 10$ in Fig. 7(a)] and later the emergence of streaky structures [cf. the u perturbation at $t \approx 30$ in Fig. 7(b)].

Figure 7 reveals that for $f \leqslant 0.036$, transition is induced in spite of the lower amplitude of the oblique modes compared to the single phase flow. This clearly points to the importance of the additional forcing induced by the inertial particles and is confirmed by the data in Fig. 8(a): Here it is demonstrated that the (1,2) mode initiated by the particle forcing is responsible for the laminar-turbulence transition at the lowest values of f. At larger values of the mass fraction, the decrease in the amplitude of the oblique modes delays the streak generation and the following breakdown, as shown in Fig. 8(b) where the particle-laden flow will eventually return to the laminar state.

D. Particle concentration

Inertial particles are shown to display a characteristic accumulation at the wall in turbulent flows: the so-called turbophoresis [46,47]. It is observed that the accumulation reaches a maximum for intermediate values of the Stokes number, about 25 in wall units, while it is zero for passive tracers [40,48]. Turbophoresis is less pronounced when simulations include a feedback on the flow and for increased mass fraction [49].

Here we examine how particle accumulation occurs during transition and the differences between the two scenarios considered. The normalized wall-normal concentration profiles, normalized with the particle number, are reported in Figs. 9 and 10 for low and large mass fraction, respectively. In each figure, the left panel displays data pertaining to the SV1 scenario, whereas the OW results are depicted on the right. Note that only a half-channel is represented in each figure since we found a symmetric distribution. For all cases under consideration, the initial amplitude is chosen to be above the critical threshold for transition to turbulence, and the time of transition is approximately 100 time units. The data for the

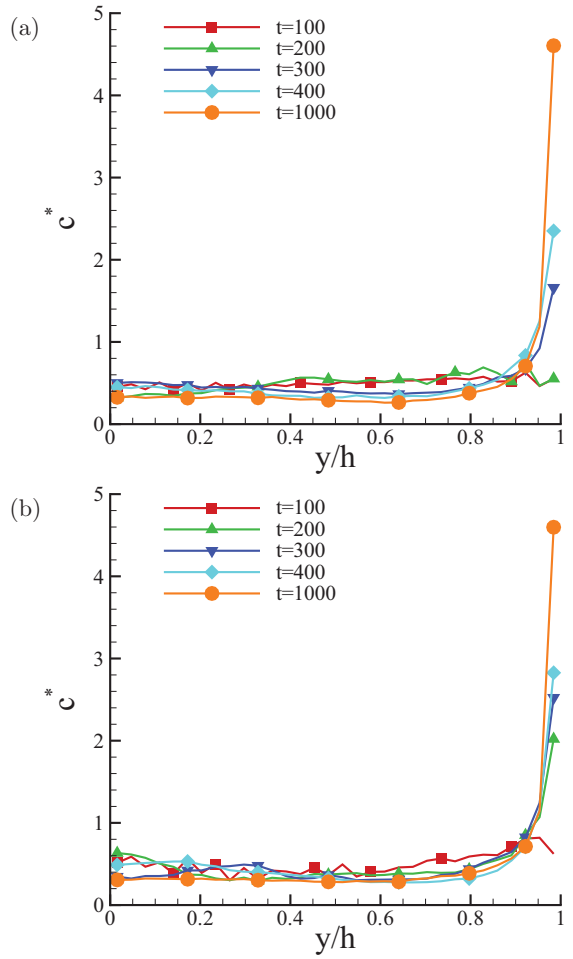

FIG. 10. (Color online) Time evolution of normalized particle concentration for (a) SV scenario and (b) OW scenario for particle mass fraction $f = 0.39$ and initial amplitude just above the threshold for transition to turbulence. $SR = 5$ and $R = 2000$. Transition to turbulence occurs at $t \approx 100$ for both scenarios.

latest time reported, $t = 1000$, clearly show the turbophoresis mentioned above, although the statistics are not yet stationary: Longer computational times would be required for steady state, especially at the lowest mass fraction.

Comparing the left and right panel of each figure one can immediately note that the drift towards the wall is initiated earlier in the case of OW scenario, while the initial uniform distribution is still visible for the SV1 scenario. This difference can be explained by the fact that the SV1 scenario is characterized solely by the streak breakdown, and this is localized in the regions of large shear towards the center of the channel. The streak formation induced by the initial streamwise vortices does not induce a variation of the mean wall-normal concentration, but rather a spanwise redistribution. Conversely, the initial stages of the OW transition are associated to the generation of streamwise vortices by nonlinear interactions, and these appear to induce a larger mixing of particles. Figures 9 and 10 also reveal that particles accumulation is more pronounced at lower mass fraction, in agreement with previous observations in turbulent flows.

IV. DISCUSSION AND CONCLUSION

Direct numerical simulations of transition in a particle-laden channel flow are performed, with particles assumed to be spherical and heavier than the fluid. The interaction between the particles and the fluid is therefore modeled by the Stokes drag as the only interaction term. The fluid flow is computed on a Eulerian mesh with Lagrangian tracking of particles. The numerical results are shown to reproduce linear stability predictions based on a continuum model.

We study subcritical transition in plane Poiseuille flow and quantify the effect of particles on the initial energy needed to reach the turbulent regime. Previous studies [13] indicate that the linear nonmodal lift-up mechanism, responsible for the amplification of streamwise-independent streaks induced by counterrotating streamwise vortices, is the dominant instability mechanism at subcritical conditions as for single phase channel flow. This is hardly affected by the presence of particles, unlike modal stability; this was explained by the disparity between the particle relaxation time and the long time scales typical of streak transient growth, at least for values of particle size and density consistent with our model. The aim of the present paper is therefore to assess whether particles influence the nonlinear stages of transition and whether this may have a relation to drag reduction observed in turbulent particle-laden shear flows. It is relevant to recall here that secondary instabilities compete against viscous diffusion of the streak [31], so that streaks need to have sufficiently high amplitudes for sufficiently long times and streamwise-dependent modes need time to reach amplitudes at which turbulent breakdown can occur. The time needed to reach these high-enough amplitudes is related to the disturbances' initial amplitude and not only to the streak amplitude.

We consider two classic transition scenarios: the SV scenario, induced by streamwise vortices and a relatively weak streamwise dependent mode, and oblique transition, OW, induced by a pair of symmetric oblique waves. In the latter, the nonmodal growth of streaks is induced by the nonlinear interaction of the two streamwise-dependent modes. The oblique scenario is known to be more effective and require lower initial disturbance energy [19,28]. To appreciate the differences between the two scenarios, the energy threshold for transition is reported in Fig. 11, normalized with the value

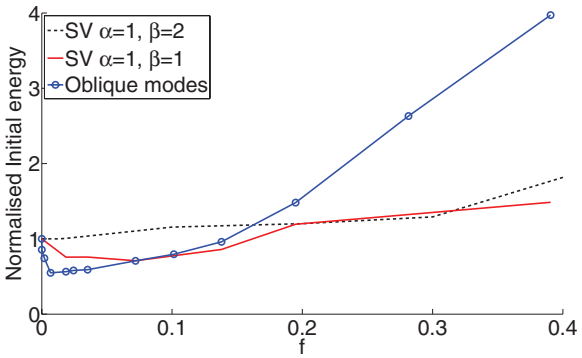

FIG. 11. Comparison between the threshold energies for the two SV scenarios and OW transition, all normalized with their energy threshold of a clean fluid.

for the corresponding single phase fluid. In the case of oblique scenario and transition initiated by streaks and the (1,1) mode, we see a small decrease of the energy threshold at the lowest particle concentrations. This is explained by the fact that in this case streaks and oblique modes are weakly affected by the particles, while these induce additional forcing of most detrimental scales that is able to trigger streak secondary instabilities. Indeed, particles induce perturbations of wave vector (1,2) (see Figs. 4 and 8), and these induce transition with lower disturbance energy. When the (1,2) mode is introduced in a controlled way in the flow (disturbance fluid velocity), transition is always delayed in the presence of particles.

For larger particle mass fraction, we observe an increase of the energy threshold, most pronounced for the oblique scenario. This is attributed to the stabilizing effect particles have on the oblique modes, an effect quantified by the nonmodal analysis of the evolution of these modes reported in Fig. 5. This stabilization is more effective in case of oblique transition since it acts directly to hinder the generation of streamwise vortices by nonlinear interactions of these oblique modes. The streak generation is delayed and weakened when the oblique modes decay faster.

In the SV scenario, the streak evolution is basically unaffected by the presence of the particles. Particles act to weaken the oblique mode and therefore delay the transition process. Results obtained with the same initial disturbance amplitude, above the critical threshold, reveal that the most evident effect of particles on the transition is that it occurs at later times: The secondary instability is initiated by lower amplitude oblique modes and requires more time to develop.

One can speculate that the results presented here can have implications for turbulent flows where drag reduction is observed for relatively large mass fraction. In Refs. [50,51], a regeneration cycle is proposed to underlie wall-bounded turbulent flows; see Fig. 12. This consists of three steps: (1) generation of streaks induced by streamwise vortices, (2) streak breakdown via secondary instabilities, and (3) regeneration of elongated vortices by nonlinear interactions between oblique modes originating at the streak breakdown. As shown in Ref. [13], the streak generation occurs on a time scale too long for particles to have an effect. However, the present investigation indicates that particles can affect this cycle in two ways. They may significantly hinder the last of these three processes, namely, the regeneration of streamwise vortices by nonlinear interactions. Indeed, the first step of the oblique scenario is the most affected in the presence of heavy particles. However, particles also induce a significant time delay on the streak breakdown (stage 2). This time delay can break the regeneration cycle. This delay can also create phases of hibernating turbulence as observed in polymer solutions. Unlike polymer suspensions, where elastic effects damp streamwise vortices [52], we see here a strong effect on the nonlinear regeneration of these vortices.

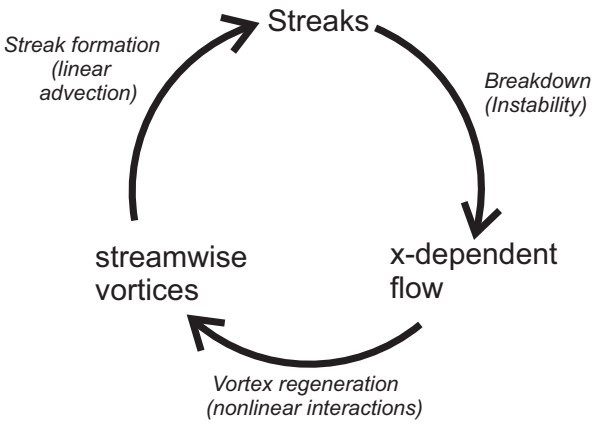

FIG. 12. Sketch of the regeneration cycle of wall turbulence; see Refs. [50,51].

The present work can be extended in several interesting ways. While here we isolated basic linear and nonlinear process, in particular, streak generation by lift-up, regeneration of streamwise vortices, and streak breakdown, the behavior of a turbulent flow can be analyzed to identify those features suggested here, such as intervals of low-activity turbulence with weak streamwise vortices and streaks of nearly nonexistent streamwise variations [26]. The effect of finite size particles also deserves considerations. In particular, our results seem to suggest that fewer neutrally buoyant large particles (low mass fraction and large Stokes numbers) can destabilize the flow as shown in the experiments by Matas *et al.* [11].

ACKNOWLEDGMENTS

The authors wish to acknowledge the contribution of Michel van Hinsberg and Philipp Schlatter to the implementation of the two-way coupling algorithm in the existing spectral code. The computations were performed thanks to computer time provided by the Energy Technology group at Thermo Fluids Engineering, TU/Eindhoven, and by SNIC (Swedish National Infrastructure for Computing).

APPENDIX: EFFECTS OF GRAVITY

In this paper we examined the effect of dispersed particles on laminar-turbulence transition aiming also to understand the phenomenon of turbulence drag reduction in turbulent channel flow. As this effect, first observed in experiments [4,6], has been reproduced in numerical simulations neglecting gravity [7], we have so far also neglected particle sedimentation to be able to isolate the effect of Stokes drag in the particle-fluid interaction.

As gravity is inevitable in our environment and we are considering heavy particles, sedimentation is strongly affecting the particle motion, especially when the flow is laminar and there is no turbulence to resuspend the particles. We therefore present in this appendix results of numerical simulations performed including gravity. These are meant to provide indications about the effect of gravity on transition, further analysis being left as future work. In the presence of gravity a new nondimensional parameter needs to be considered, the Froude number $\mathrm{Fr} = U/\sqrt{gL}$ with g the gravitational acceleration. Note that the friction Reynolds number changes in the case of vertical channels: It is 106 for the downward flow, whereas it reduces to 88 for the upward flow.

The time evolution of the total streamwise and wall-normal perturbation velocity are depicted in Fig. 13 for both the SV and OW scenarios at fixed initial disturbance energy chosen

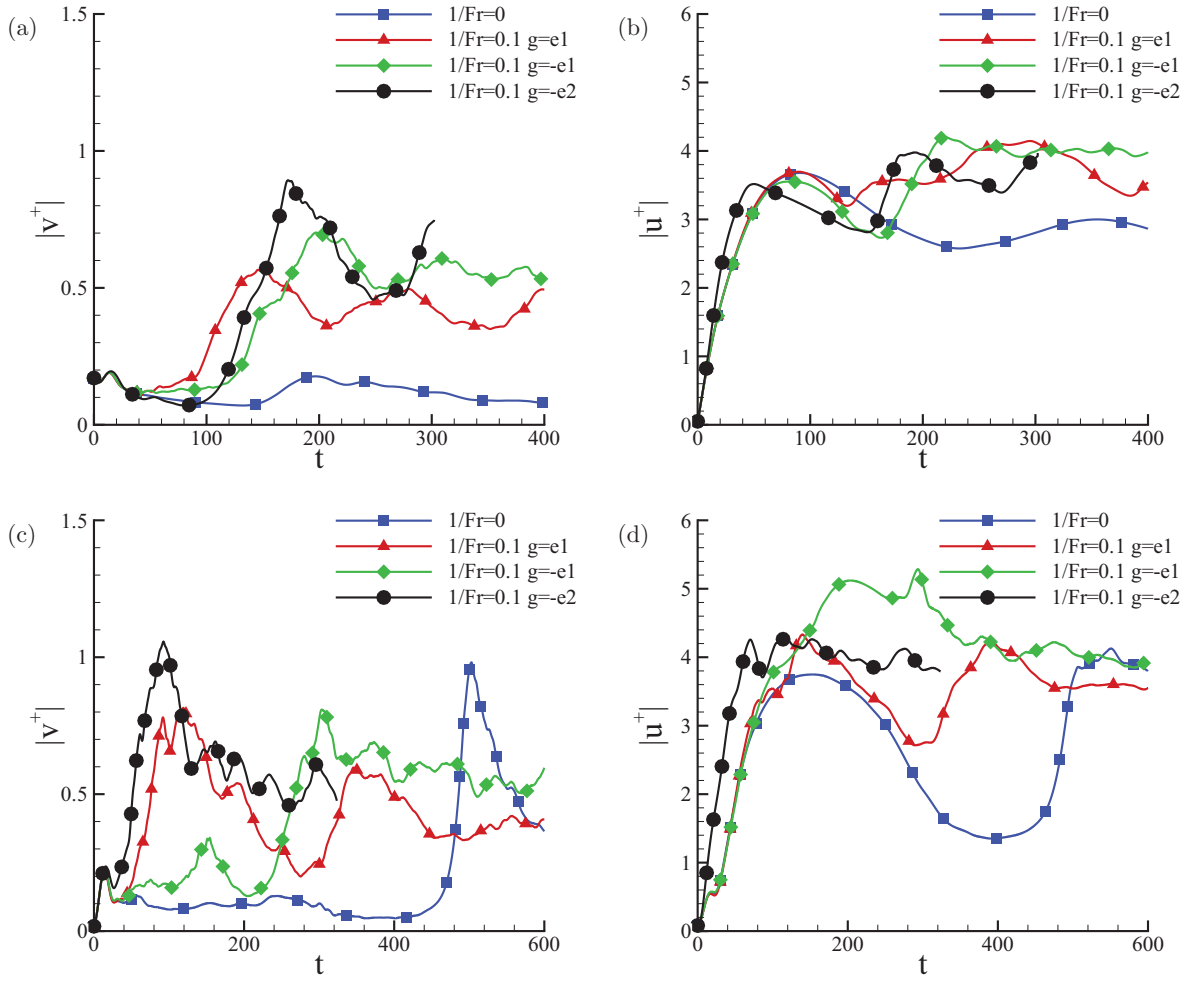

FIG. 13. (Color online) Volume integral of the wall-normal velocity (a, c) and streamwise velocity (b, d) perturbation as a function of time for Froude number Fr $= 10, \infty$ and gravity orientations. (a, b) Streamwise vortices scenario, initial disturbance energy $E = 1.37 \times 10^{-3}$. (c, d) Oblique waves scenario. Initial disturbance energy $E = 3.65 \times 10^{-4}$.

to be close to the threshold transition amplitude for the case without gravity. The mass load $f = 0.2$ and results for two values of Fr are reported, Fr $= 10, \infty$, the first corresponding to a channel with velocity of 3.42 m/s and half-height of 1.17 cm and the second corresponding to no gravity. In the figure legend we denote by e_2 the wall normal direction and by e_1 the streamwise, so that $g = -e_1$ indicates cases where gravity acts against the flow direction. From the data in the figure it is possible to see that the action of gravity facilitates the turbulent-laminar transition independently of the direction in which gravity is acting. When the Froude number is large, i.e., low channels and/or low velocities, the transient growth of streaks is similar to the zero gravity scenario when the gravity acts in the streamwise direction and early transition is caused by an increase of the wall-normal (and cross-stream) velocity perturbation. Horizontal channels display a quite different behavior as particle sedimentation breaks the wall-normal symmetry of the flow and delays the growth of streamwise streaks. However, more intense cross-stream disturbances still induce early transition.

[1] P. J. Schmid and D. S. Henningson, *Stability and Transition in Shear Flows* (Springer, New York, 2001).
[2] B. A. Toms, in *Proceedings of First International Congress on Rheology* (North-Holland, Amsterdam, 1949), Sec. II, pp. 135.
[3] J. S. Paschkewitz, Y. Dubief, C. D. Dimitropoulos, E. G. Shaqfeh, and P. Moin, J. Fluid Mech. **518**, 281 (2004).
[4] W. T. Sproull, Nature (London) **190**, 976 (1961).
[5] P. G. Saffman, J. Fluid Mech. **13**, 120 (1962).
[6] S. J. Rossetti and R. Pfeffer, AIChE J. **18**, 31 (1972).
[7] L. H. Zhao, H. I. Andersson, and J. J. J. Gillissen, Phys. Fluids **22**, 081702 (2010).
[8] F. Toschi and E. Bodenschatz, Annu. Rev. Fluid Mech. **41**, 375 (2009).

[9] S. Balachandar and J. K. Eaton, Annu. Rev. Fluid Mech. **42**, 111 (2009).
[10] M. R. Maxey and J. J. Riley, Phys. Fluids **26**, 883 (1983).
[11] J. P. Matas, J. F. Morris, and E. Guazzelli, Phys. Rev. Lett. **90**, 014501 (2003).
[12] J. P. Matas, J. F. Morris, and E. Guazzelli, Phil. Trans. R. Soc. Lond. A **361**, 911 (2003).
[13] J. Klinkenberg, H. C. de Lange, and L. Brandt, Phys. Fluids **23**, 064110 (2011).
[14] J. Klinkenberg, H. C. de Lange, and L. Brandt, Meccanica (unpublished).
[15] T.M. Schneider, B. Eckhardt, and J.A. Yorke, Phys. Rev. Lett. **99**, 034502 (2007).
[16] M. Nagata, J. Fluid Mech. **217**, 519 (1990).
[17] F. Waleffe, Phys. Rev. Lett. **81**, 4140 (1998).
[18] F. Waleffe, J. Fluid Mech. **435**, 93 (2001).
[19] Y. Duguet, L. Brandt, and B. R. J. Larsson, Phys. Rev. E **82**, 026316 (2010).
[20] J. Wang, J. Gibson, and F. Waleffe, Phys. Rev. Lett. **98**, 204501 (2007).
[21] G. Kawahara, Phys. Fluids **17**, 041702 (2005).
[22] Y. Duguet, C. C. T. Pringle, and R. R. Kerswell, Phys. Fluids, **20**, 114102 (2008).
[23] Y. Duguet, A. P. Willis, and R. R. Kerswell, J. Fluid Mech. **613**, 255 (2008).
[24] B. Eckhardt, T. M. Schneider, B. Hof, and J. Westerweel, Annu. Rev. Fluid Mech. **39**, 447 (2007).
[25] P. A. Stone, F. Waleffe, and M. D. Graham, Phys. Rev. Lett. **89**, 208301 (2002).
[26] L. Xi and M. D. Graham, J. Fluid Mech. **647**, 421 (2010).
[27] L. Xi and M.D. Graham, Phys. Rev. Lett. **104**, 218301 (2010).
[28] S. C. Reddy, Peter J. Schmid, J. S. Baggett, and D. S. Henningson, J. Fluid Mech. **365**, 269 (1998).
[29] L. N. Trefethen, A. E. Trefethen, S. C. Reddy, and T. A. Driscoll, Science **261**, 578 (1993).
[30] S. C. Reddy and D. S. Henningson, J. Fluid Mech. **252**, 209 (1993).
[31] W. Schoppa and F. Hussain, J. Fluid Mech. **453**, 57 (2002).
[32] C. Cossu, L. Brandt, S. Bagheri, and D. S. Henningson, Phys. Fluids **23**, 074103 (2011).
[33] P. J. Schmid and D. S. Henningson, Phys. Fluids **4**, 1986 (1992).
[34] S. Berlin, A. Lundbladh, and D. S. Henningson, Phys. Fluids **6**, 1949 (1994).
[35] D. Ponziani, C. M. Casciola, F. Zirilli, and R. Piva, Stud. Appl. Math. **105**, 121 (2000).
[36] S. Cherubini, P. DePalma, J. C. Robinet, and A. Bottaro, Phys. Rev. E **82**, 066302 (2010).
[37] A. Monokrousos, A. Bottaro, L. Brandt, A. Di Vita, and D. S. Henningson, Phys. Rev. Lett. **106**, 134502 (2011).
[38] P. N. Rowe and G. A. Enwood, Trans. Inst. Chem. Eng. **39**, 43 (1962).
[39] M. Chevalier, P. Schlatter, A. Lundbladh, and D. S. Henningson, Technical Report TRITA-MEK 2007:07, Royal Institute of Technology (KTH), Dept. of Mechanics, Stockholm, 2007.
[40] G. Sardina, P. Schlatter, L. Brandt, F. Picano, and C. M. Casciola, J. Fluid Mech. **699**, 50 (2012).
[41] J. K. Eaton, Int. J. Multiphase Flow **35**, 792 (2009).
[42] P. Gualtieri, F. Picano, G. Sardina, and C. M. Casciola, J. Fluid Mech. **715**, 134 (2013).
[43] J. Klinkenberg, Licentiate thesis, KTH, Royal Institute of Technology, Stockholm, 2011.
[44] P. Moin and K. Mahesh, Annu. Rev. Fluid Mech. **30**, 539 (1998).
[45] S. Toh and T. Itano, J. Fluid Mech. **481**, 67 (2003).
[46] M. Caporaloni, F. Tampieri, F. Trombetti, and O. Vittori, J. Atmos. Sci. **32**, 565 (1975).
[47] A. Soldati and C. Marchioli, Int. J. Multiphase Flow **35**, 827 (2009).
[48] G. Sardina, F. Picano F., P. Schlatter, L. Brandt, and C. M. Casciola, Flow Turb. Comb. **86**, 519 (2011).
[49] L. M. Portela and R. V. A. Oliemans, Intl J. Numer. Meth. Fluids **43**, 1045 (2003).
[50] J. M. Hamilton, J. Kim, and F. Waleffe, J. Fluid Mech. **287**, 317 (1995).
[51] F. Waleffe, Phys. Fluids **9**, 883 (1997).
[52] Y. Dubief, C. M. White, V. E. Terrapon, E. S. G. Shaqfeh, P. Moin, and S. K. Lele, J. Fluid Mech. **514**, 271 (2004).